Energy and Buildings 130 (2016) 228–237

Contents lists available at ScienceDirect

Energy and Buildings

journal homepage: www.elsevier.com/locate/enbuild

Deformation and thermal resistance study of aerogel blanket insulation material under uniaxial compression

Atiyeh Hoseini, Ali Malekian, Majid Bahrami*

Laboratory for Alternative Energy Conversion, School of Mechatronic Systems Engineering, Simon Fraser University, 250-13450 102 Avenue, Surrey, British Columbia, V3T 0A3, Canada

ARTICLE INFO

Article history:
Received 13 June 2016
Received in revised form 15 August 2016
Accepted 17 August 2016
Available online 18 August 2016

Keywords:
Aerogel blanket
Thermal insulation material
Heat flow meter
Thermomechanical analyzer
Modeling
Compression
Experiment

ABSTRACT

Aerogel based composite insulation materials have very low thermal conductivity (~0.016 to ~0.040 $W m^{-1} K^{-1}$). Aerogel blankets are flexible; however, compressive loads may affect their thermal resistance due to their porous nature. In this paper, the thermal resistance and mechanical deformation of aerogel blankets were studied under compressive mechanical loading. The R-values of two types of commercially available aerogel blankets (Cryogel®Z and ThermalWrap™) were measured using a heat flow meter (HFM) under compressive loads up to 8 kPa. Additionally, a mechanistic analytical model was developed to predict the deformation of aerogel blankets using their microstructural properties, including average fiber diameter, particle diameter and porosity. The bending of fibers was considered as the main deformation mechanism at the unit cell level, and the overall blanket deformation was calculated from the summation of the deformations of all the unit cells. The stress-strain relationship was verified using the results of the experimental studies conducted with a HFM and a thermomechanical analyzer (TMA). The maximum decrease in thickness was 20% for 8 mm ThermalWrap™ and the maximum change in R-value was a 10% increase with compression observed for a 10 mm Cryogel®Z. The results indicated that aerogel blankets remain remarkably effective thermal insulation materials under compression. Even after 20 compression-decompression loading cycles, the reduction of thermal conductivity was ≤5%, and the permanent deformation was ≤6%.

1. Introduction

A staggering 64% of household energy use and 53% of commercial energy use in Canada were for heating and cooling purposes, according to data from year 2009 [1]. Using more efficient thermal insulation system in buildings is a feasible approach to reduce energy demand as a result of reduced energy losses [2].

The thermal performance of insulation materials is typically judged by their R-value (thermal resistance value) determined by standardized tests, such as ASTM C177 and C518; however, the in-service R-value may differ for several reasons. For instance, R-value decreases when porous material is compressed. The thermal resistance of insulations may also vary with temperature and presence of moisture. These R-value variations are material specific and not linear. Among available insulating material categories, aerogels are high performance insulations for both stationary and mobile applications.

Aerogels are highly porous materials with large surface area and pore volume. They have a low density and high porosity (>90%), which makes them super thermal insulators [3] or great additives to enhance the insulation performance of the composites such as aerogel based plasters[4]. The highly porous structure of aerogels is formed by sol gel chemistry [5]. Although they have outstanding thermal insulating properties, the cost and weak mechanical strength of aerogels have limited their use. One method of reinforcing aerogels is combining aerogel with a fibrous matrix that supports the aerogel particles to create a composite called an aerogel blanket [6]. Aerogel blankets are flexible, highly porous thermal insulators, which have remarkably high thermal resistance [5]. In this paper, aerogel blanket super insulation is studied under compressive mechanical loading to investigate the effect of uniaxial compression on its thermal performance and structural deformation.

Yarbrough et al. [7] studied the reduction of thermal resistance of loose-fill insulations due to mechanical compression and measured the thickness reduction as a function of applied load for samples of fiberglass batt, 1oose-fill fiberglass, loose-fill rock wool, and loose-fill cellulosic insulation. Their results showed that the low density materials were affected the most showing up to 40% thickness decrease under 0.14 kPa load. Also, they showed that reduction in thermal resistance under compression was greatest

* Corresponding author.
E-mail address: mbahrami@sfu.ca (M. Bahrami).

http://dx.doi.org/10.1016/j.enbuild.2016.08.053
0378-7788/

Nomenclature

A	Area (m^2)
D	Diameter (m)
ε	Porosity
e	Strain
δ	Deformation (m)
EI	Flexural rigidity ($N\,m^2$)
γ	Stress (kPa)
F	Force (N)Force (N)
k	Thermal conductivity ($W\,m^{-1}\,K^{-1}$)
a	Aerogel particle layer
l	Length (m)
App	Apparent
t	Thickness (m)
b	Blanket
N	Number
$Cond$	Conduction
$\dot{q}$	Heat flux ($W\,m^{-2}$)
eff	Effective
R_{total}	Total thermal resistance ($m^2\ K\,W^{-1}$)
F	Fiber
r	Radius (m)
G	Gas
T	Temperature (K)
Gs	Gas solid region
V	Volume (m^3)
Sm	Solid medium
lp	Large particle
tot	Total
u_{tot}	Unit cell total

for the fiberglass insulations (~20% under 0.14 kPa load). Adams and Hust [8] investigated the reduction of thermal conductivity under compression for five common porous insulation products; cellulose, rock/slag wool, bonded and unbonded glass fiber, and a glass fiber blanket. Graves and Yarbrough [9] measured the R-values of six commercially available fiberglass batts at their full thickness and compressed to 50% of full thickness, following ASTM C518 test methods. They observed that the decrease in thermal resistance during compression was greater for samples with higher density (compression to 50% of full thickness of higher density products reduced the R-value by 45%). Symons et al. [10] studied blanket form materials, e.g. low density fiberglass, sheep's wool and polyester fiber, as well as loose-fill form materials, e.g. cellulose fiber, sheep wool and rock wool, following ASTM C518 standards. Their results showed that of the materials tested, the fiberglass blankets had the lowest thermal conductivity (~0.032 $W\,m^{-1}\,K^{-1}$), requiring less thickness (~80 mm) to achieve target thermal resistance values of 2.5 $m^2\,K\,W^{-1}$ for a building in Australia. Kolich et al. [11] studied the thermal and physical properties of internal car insulation materials at −20 °C to 60 °C and 0% to 60% compression. They determined specific heat of their samples, following ASTM E1269-05, and their volume density using ASTM C302-95. They also correlated increases in apparent thermal conductivity of uniform porous materials with increasing density, and found that the apparent thermal conductivity of laminated materials (e.g. foam plastic-leader) decreased with increasing density, which was caused by variation in the shape of the pores. There are few studies on the relationship between thickness, compression, deformation and thermal performance of aerogel based composite insulation materials. A summary of available studies on aerogel composites is presented in Table 1.

Our literature review indicates that the effect of compression on the thermal performance and structural deformation of aerogel blankets has not been thoroughly studied yet. Silica aerogel can crack and separate from the fibrous matrix, which affects the thermal resistance of the aerogel blanket insulation. The objective of this study is to measure the thermal performance of two types of aerogel blanket samples under compression and after repeated mechanical load cycling. Additionally, a mechanistic analytical model is developed, following a unit cell approach, for predicting the deformation of the aerogel blankets as a function of compressive mechanical load. Bending of fibers is considered as the main deformation mechanism at the unit cell level and the overall blanket deformation is calculated from the summation of the deformations of all the layers. Employing the proposed model, a compact relationship between compressive strain and applied load (stress) is presented, which is verified using the experimental data that can be employed in predicting the deformation of the fibrous insulation materials at particular density.

2. Experimental

Samples of four aerogel blanket insulation materials, 5 mm and 10 mm thick Cryogel®Z (CZ) and 5 mm and 8 mm thick ThermalWrap™ (TW), were obtained from Aspen Aerogel and Cabot Corporation, respectively. The sample specifications are summarized in Table 2.

A thermomechanical analyzer (TMA) (Q400EM, TA Instruments) with a macro-expansion probe with a 6.07 mm diameter contact area was used to compress 7 mm × 7 mm insulation samples. Two samples of each of type of the aerogel blanket insulations were tested with linear ramp force up to 0.4 N in a dry nitrogen environment at room temperature. A schematic of the TMA instrument is shown in Fig. 1. TMA measures sample displacement at various temperatures, time and applied forces and its resolution for displacement is less than 0.5 nm.

The thermal resistance of typical insulation materials decreases with compression. Therefore, it is essential to control sample compression during thermophysical property testing. A heat flow meter (HFM 436/3/1 Lambda, NETZSCH), shown schematically in Fig. 2, was employed to measure the thermal conductivity (k-value) and R-value of aerogel blankets over a range of compression. HFM precisely regulates compression and can test samples with controlled loads up to 21 kPa while measuring sample thickness. Insulation samples (30.5 cm × 30.5 cm) were tested between two heat flux sensors under a specific temperature gradient applied by a hot plate and cold plate. The total thermal resistance was calculated from the equilibrium temperature difference across sample and the known heat flux applied to the sample. Further details of the apparatus and the methodology used in the thermal resistance measurements can be found in ASTM C518 [19].

Aerogel blanket samples were also imaged with Aspex Explorer scanning electron microscope to study the fiber-particle arrangement in the blankets. The changes in the morphology of the material under compression were also evaluated by SEM. For this, samples were pressed up to a predetermined load at room temperature, which was the maximum load applied on the samples using HFM and TMA, and the images were taken under no-load and compressed conditions. Under SEM, the material does not show any noticeable difference from its original state, Fig. 3.

3. Model development

SEM images of the aerogel blankets revealed a repetitive microstructural arrangement of fibers and aerogel particles leading to a unit cell approach for this analytical model. Fig. 4(a), (b) and (c)

Table 1
Summary of available studies on thickness or density of aerogel based composites.

Author(s)	Notes
Erdem Cuce et al. [12]	• Investigated optimum thickness of aerogel blanket insulation to maximize energy saving and thermal comfort. • Determined dependency of annual energy use on insulation thickness.
Gupta and Ricci [13]	• Fabricated aerogel/epoxy composites. • Studied the composites (density of 980 and 1070 kg m^{-3}) under compressive loads (0–120 MPa). • Observed some cracks but no strength loss at 25% compressive strain.
Bardy et al. [14]	• Tested samples of prototype and product-line aerogel insulating blankets for thermal conductivity and compressive strain at incremental loads up to 1.2 MPa. • Found that the prototype sample has higher resistance under compression and recovers to its original thickness upon decompression.
Duoqi Shi et al. [15]	• Fabricated ceramic-fiber- reinforced SiO_2 aerogel. • nvestigated the composite properties under compression (up to 1.5 MPa for in-plane and 16 MPa for out-of-plane compression) at high temperatures (up to 900 °C). • Found that in-plane Young's modulus increases with temperature, but out-of-plane modulus decreases with temperature.
Wu et al. [16]	• Fabricated multilayer fiber-reinforced aerogel composites using glass fiber and SiO_2 aerogel. • Used unit cell approach to model the conductive heat transfer in the composite. • Improved the mechanical strengths of the aerogel composites via impregnating multilayer aligned fibers into aerogels. • Studied the effect of fiber alignments on the compressive and bending strengths and thermal conductivity of the composites.
Neugebauer [17]	• Reduced the thermal conductivity of a bed of granular aerogels through compression. • Suggested that by controlling the load on the beds of granular aerogels, higher thermal resistance can be achieved.

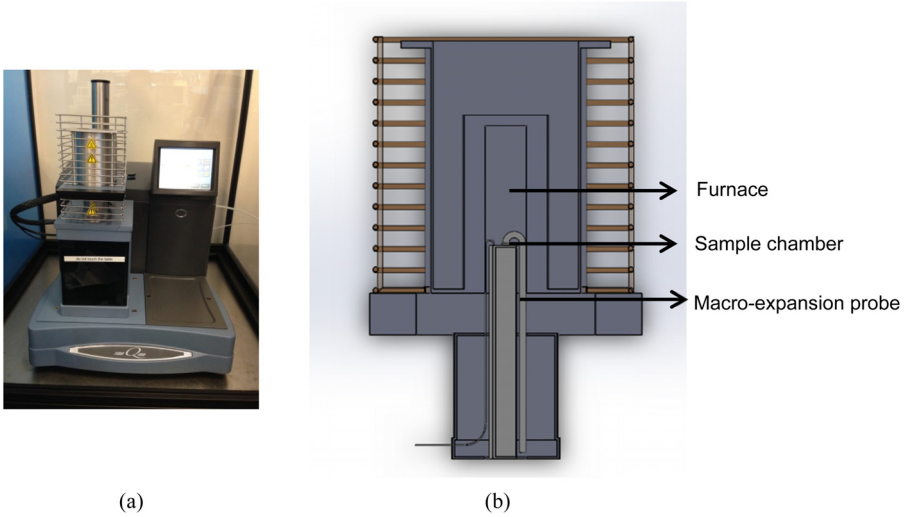

Fig. 1. TMA device (a) and its schematic (b) [18].

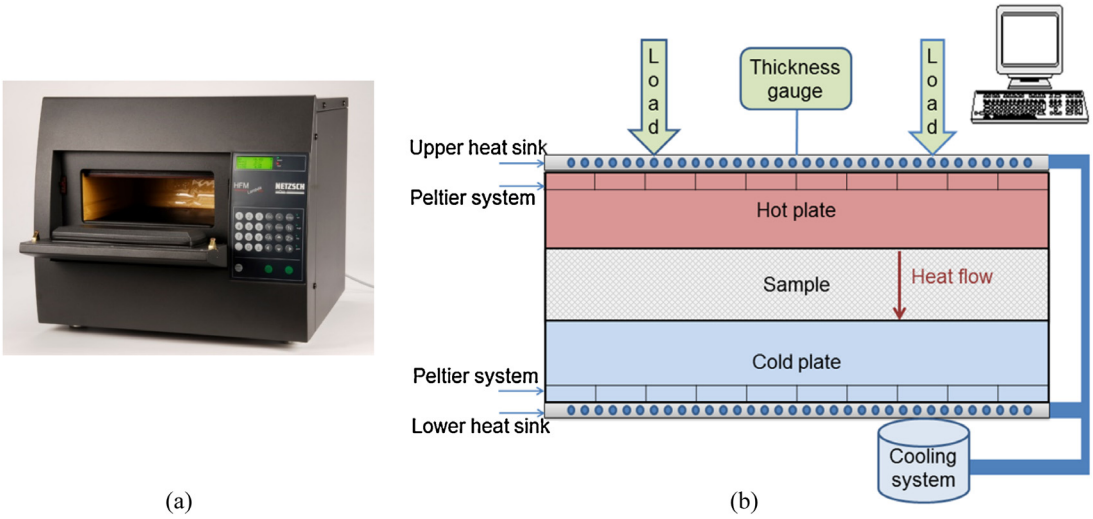

Fig. 2. The heat flow meter (HFM) instrument (a) and its schematic (b).

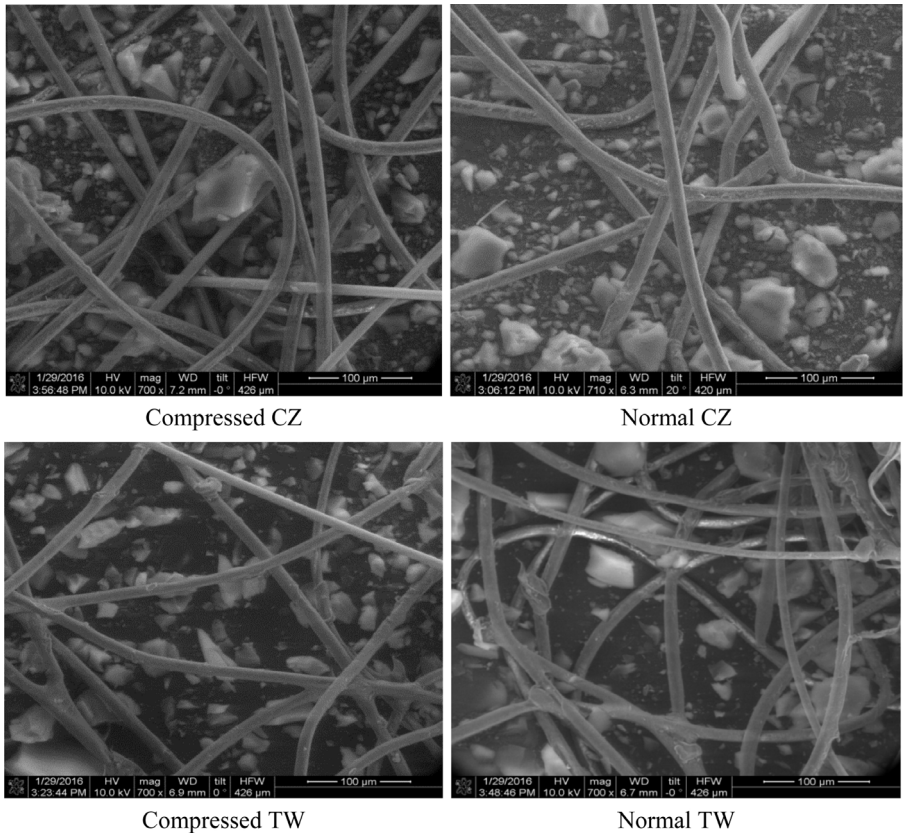

Fig. 3. Microstructure of aerogel blanket samples; at no-load and compressed conditions.

Table 2
Aerogel blanket sample specifications.

Sample specification	Cryogel®Z (CZ)	ThermalWrap™ (TW)
Provider	Aspen Aerogel	Cabot Corp.
Thickness[a]	10 mm 5 mm	8 mm 5 mm
Density[a]	130 kg m^{-3}	70 kg m^{-3}
Fiber composition[a]	Polyester/fiber glass	Polyester and polyethylene
Powder material[a]	Silica (SiO_2)	Silica (SiO_2)
Thermal conductivity (@ RT)[a]	0.014 W m^{-1} K^{-1}	0.023 W m^{-1} K^{-1}
Powder diameter (aerogel layer thickness) [20]	10 μm	4 μm
Fiber diameter [20]	20 μm	7 μm
Porosity [20]	91%	79%
Fiber modulus of elasticity	85 GPa [21]	3.5 GPa [22]

[a] Manufacturer Data [23], [24].

show a SEM image of Cryogel®Z (CZ) aerogel blanket, schematics of the proposed geometric model and unit cell, respectively. This unit cell, designed to model the mechanical behavior of aerogel blanket under compression, includes fibers surrounded by small aerogel particles with a large particle at the center. Each fiber was modeled as a bending beam supported through a contact point with the fiber below. Force is applied to each fiber through a contact point with a fiber above that is one edge of the unit cell, l_f, away from the supporting contact point.

In our approach, two different porosities were considered; 1) porosity of the aerogel coating on the fibers, ε_a, and 2) porosity of the blanket, ε_b. The assumptions used in the model development are listed below:

1) Smooth sphere and fiber surfaces, i.e., no rough contacts on sphere–sphere and fiber-sphere contact points.
2) No contact point between the large particle at the center and the fiber-aerogel composite, i.e. the unit cell aspect ratio is $\frac{l_f}{D_{lp}} \geq 2$. For this assumption to be applicable, the range of the applied load should be limited to less than 10 kPa that is in the range of the load applied on such material in practice.
3) Negligible deformation for aerogel particles (Hertzian contact) compared to bending fibers deformation ($\delta_{max\_fibers} \sim 10^{10}\ \delta_{max\_particles}$).

The length of the fibers in each unit cell, l_f, is equivalent to the length of the two edges of the unit cell, and can be found from the porosities using the following equation:

$$1-\varepsilon_b = \frac{V_{solid}}{V_{total}} = \frac{\frac{3\pi}{8}{D_f}^2 l_f + \frac{3\pi}{2} l_f \left(D_f t_a + {t_a}^2\right)(1-\varepsilon_a) + \frac{4\pi}{3}\left[3\left(\frac{D_f}{2}+t_a\right)\right]^3 (1-\varepsilon_a)}{6{l_f}^2\left(\frac{D_f}{2}+t_a\right)} \quad (1)$$

where, V_{solid}, is the solid volume of the unit cell, V_{total}, is the total volume of the unit cell, D_f, is the diameter of the fibers, t_a, is the thickness of the layer of aerogel on the fibers. The third edge of the unit cell can be calculated from the fibers and aerogel layer thickness ($3 \times (D_f + 2t_a)$). From the length of the fibers and the compressive force, which is assumed to be applied on the end point of the fiber on top, the deflection of the unit cell in the z direction, can be calculated according to beam theory for beams supported on both ends and single load at the center, Fig. 5(a) [25]. Also, according to the second and third assumptions listed in Section 3, the large spherical aerogel particles are only contributing to the effective porosity of the unit cell and do not affect the total deformation,

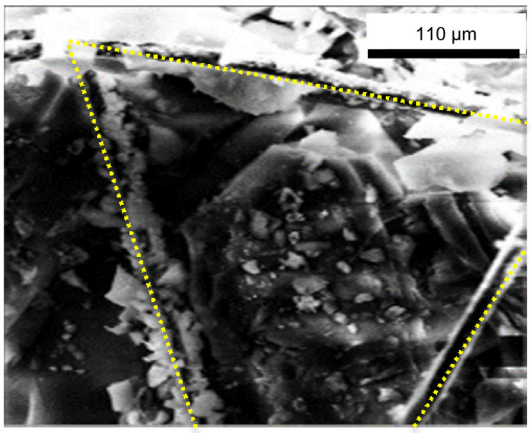

(a)

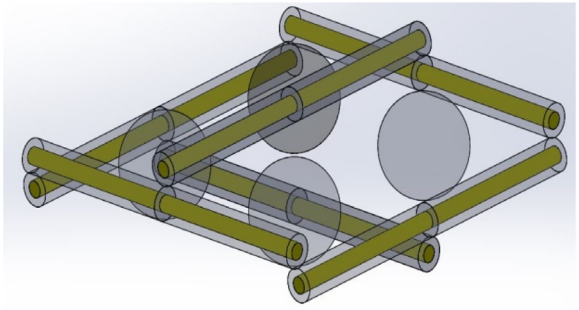

(b)

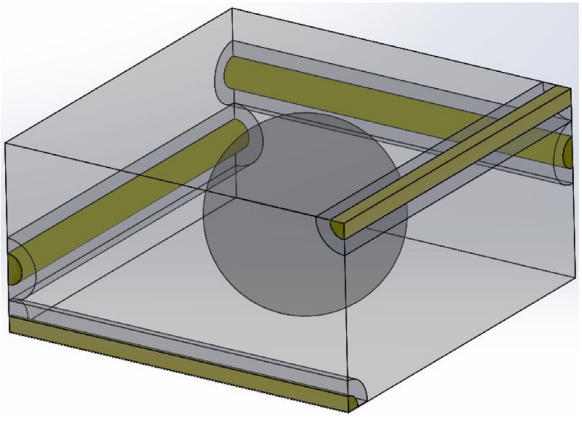

(c)

Fig. 4. SEM image of aerogel blanket (CZ) showing aerogel coated fibers (marked with dotted lines) and aerogel filled pores (a), and schematics of the proposed geometrical model for aerogel blanket (b), unit cell showing fibers coated with a layer of aerogel particles, a larger spherical aerogel particle at the center, a force, *Fi*, applied to the uppermost fiber and the fibers length in the unit cell, l_f (c).

so the stress-strain analysis is applied on the simplified unit cell, as shown in Fig. 5(b).

The unit cell deflection is calculated from Eq. (2):

$$\delta_u = 4 \times \delta_{Beam} \tag{2}$$

where the deflection of each beam, δ_{Beam}, is

$$\delta_{Beam} = \frac{F' \times {l_f}^3}{3(EI)_{eff}} \tag{3}$$

and the applied force on one unit cell is:

$$F' = \frac{F_{tot}}{N_u} \tag{4}$$

and N_u is the number of unit cells in one layer, obtained using the equation

$$N_u = \frac{A_{sample}}{{l_f}^2} \tag{5}$$

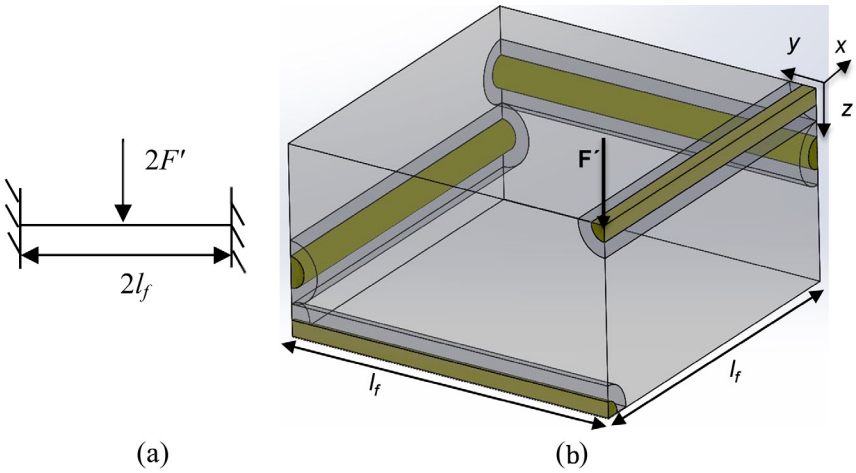

Fig. 5. Schematic of the applied beam theory (a) and the unit cell used in stress-strain analysis (b).

in which A_{sample} is area of the sample. $(EI)_{eff}$ is the effective flexural rigidity of the beam, which can be calculated using elastic modulus of fibers and aerogel particles, E, and their moment of inertia, I according to:

$$(EI)_{eff} = (EI)_{fiber} + (EI)_{aerogel} \tag{6}$$

However, the *EI* term corresponding to aerogel layer is negligible compared to fibers elasticity and thus, is not considered in the model.

In order to calculate the total deformation of an aerogel blanket, the number of layers should be multiplied by the deformation of one layer, which equals the deformation of one unit cell ($\delta_{layer} = \delta_u$). The number of layers in the through-plane direction can be calculated from:

$$N_{layers} = \frac{t_b}{6\left(\frac{D_f}{2} + t_a\right)} \tag{7}$$

where t_b is the thickness of the aerogel blanket. Since the deformation of one layer equals the deformation of one unit cell, finally, the total deformation can be reported as:

$$\delta_{tot} = N_{layers} \times \delta_{layer} \tag{8}$$

Therefore, by combining Eqs. (2)–(8), the total deformation of an aerogel blanket can be obtained from a closed form analytical relationship shown in Eq. (9):

$$\delta_{tot} = \frac{4 t_b P_{tot} {l_f}^5}{9\left(D_f + 2t_a\right)(EI)_{fiber}} \tag{9}$$

Eq. (10) is a non-dimensionalized compact relationship between the compressive strain, *e*, and mechanical load (stress), γ, presented as follows:

$$e = \gamma\left(\frac{4 {l_f}^5}{9\left(D_f + 2t_a\right)(EI)_{fiber}}\right) \tag{10}$$

Compressing aerogel blankets results in a change in its microstructure thus the porosity varies with compression. Assuming that the volume of fibers and aerogel particles (solid volume) do not change at each loading step and only the pore volume decreases, the new porosity can be calculated using the new thickness of the sample. Therefore, the expected porosity can be defined based on the relation for a change in volume, where M is the compression factor (ratio of the uncompressed blanket thickness to the compressed thickness at each loading step; i.e. $\frac{t_{b,initial}}{t_{b,new}}$ where $t_{b,initial}$ and $t_{b,new}$ are the initial and new thickness of the aerogel blanket, respectively, and ε_b is the void fraction of the aerogel blanket material ($0 < \varepsilon_b < 1$).

$$\varepsilon_{b,new} = 1 - M\left(1 - \varepsilon_{b,initial}\right) \tag{11}$$

Using Eq. (11) the new porosity can be obtained after each load increment and thickness calculation. The algorithm for this porosity modification is presented in Fig. 6.

The mentioned algorithm can be expressed in a compact relationship as follows to calculate the blanket deformation at each loading step directly, Eq. (12):

$$\lim_{n\to\infty} \delta_i = t_{b,i-1}\frac{P_{tot,i}}{n}\frac{2 l_{f_{i-1}}^5}{9(EI)_{fiber}\left(\frac{D_f}{2} + t_a\right)} \quad i = 1, \ldots, n \tag{12}$$

where $l_{f,i-1}$ has to be calculated from Eq. (13):

$$l_{f,i-1} = \frac{1}{32\left(\frac{D_f}{2} + t_a\right)\left[\frac{t_{b,initial}}{t_{b,i-1}}(1-\varepsilon_{b,initial})\right]}\pi D_f^2 + 4\pi(1-\varepsilon_a)(D_f t_a + t_a^2) + \sqrt{16\pi}\sqrt{3072(1-\varepsilon_a)\left[\frac{t_{b,initial}}{t_{b,i-1}}(1-\varepsilon_{b,initial})\right]\left(\frac{D_f}{2} + t_a\right)^4 + \pi\left(\frac{1}{4}D_f^2 + (1-\varepsilon_a)(D_f t_a + t_a^2)\right)^2} \tag{13}$$

4. Results and discussion

A new nonlinear model was developed to predict the deformation of aerogel blanket material as a function of the applied mechanical load. Figs. 7–10 present the results of the experiments performed by HFM and TMA and comparison to the developed model. The results of the proposed approach agreed well with the experimental data with low relative difference (maximum 10%) and show that compression had minimal effect on the aerogel blanket insulation materials compared to conventional insulation materials, e.g. cellulose, rock wool and fiberglass. In Ref. [7], large strain were measured under relatively low loads. The authors reported 40% strain in fiberglass, 26% strain in rock wool and 20% strain in cellulosic insulation material, after applying maximum of 0.14 kPa on the samples with initial thickness of 30 cm.

Fig. 11 demonstrates the experimental measured thermal resistance for all the samples as a function of their thickness under various loading conditions. The R-values were obtained at reduced thicknesses without removing the insulation specimen from the HFM. The maximum load that HFM can apply on samples depends on two factors: 1) the compression load cannot be greater than

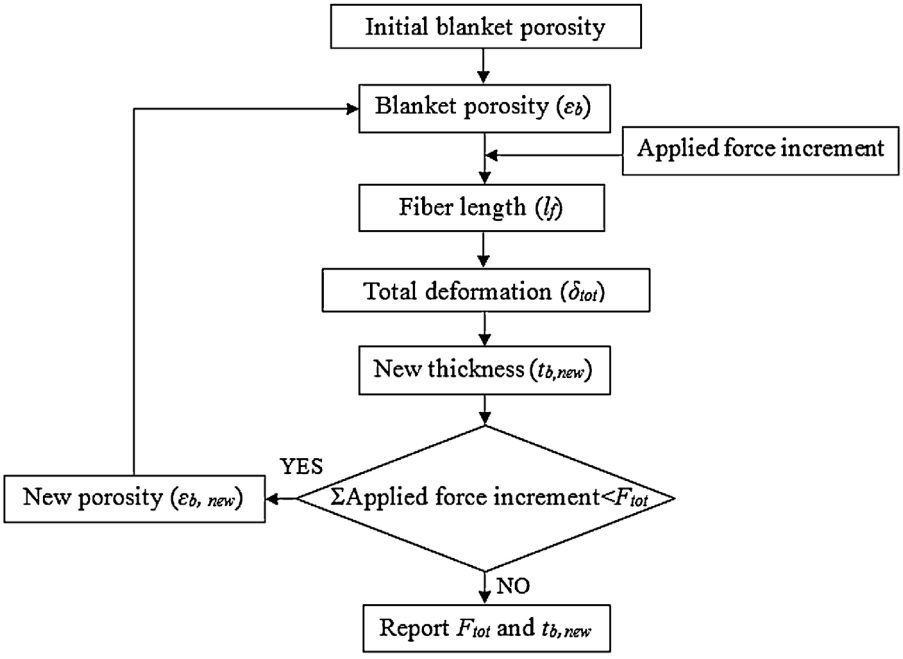

Fig. 6. Porosity modification algorithm.

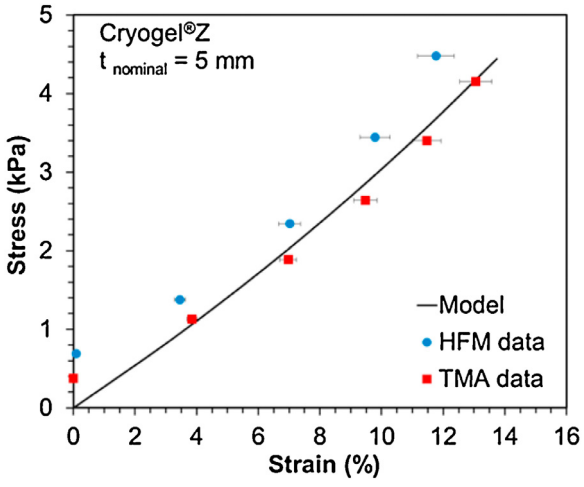

Fig. 7. Experimental stress-strain data and modeling result for CZ sample of 5 mm nominal thickness.

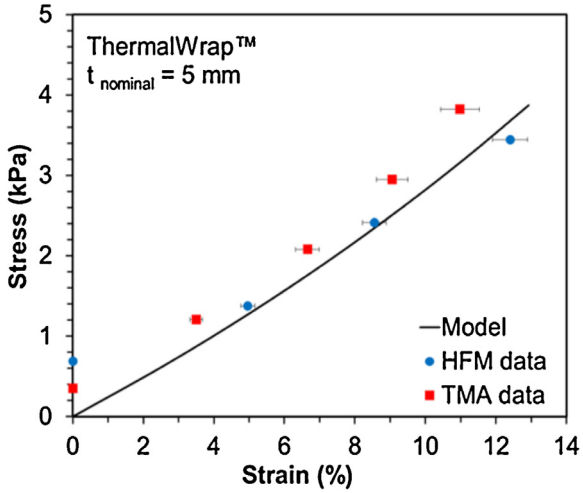

Fig. 8. Experimental stress-strain data and modeling result for TW sample of 5 mm nominal thickness.

21 kPa; 2) the combined thickness of the specimen, the heat flux transducer and any damping material, which in total equals the distance between the cold and hot plates, must be controlled to be large enough in order to minimize the effect of edge losses on the measurement of heat flux [19]. Each specimen was tested under increasing loads to the minimum allowed sample thickness. The standard deviation of the total resistances determined from the experimental results were less than 10^{-4} m^2 °C W^{-1}. The relationship between total thermal resistance, thickness and the effective thermal conductivity is as follows:

$$R_{tot_i} = \frac{t_{b,i}}{k_{eff} \cdot A_{sample}} \quad i = 1, 2 \quad (13)$$

where k_{eff} represents the effective thermal conductivity and A_{sample} is the surface area of the sample in contact with the plates, respectively.

The relationship for predicting the deformation of aerogel blanket can be extended to predict the thermal resistance of the samples at various compressions (Eq. (13)). The thickness can be calculated having the deformation and porosity at each loading and for the thermal conductivity the analytical relationship for calculating the thermal conductivity of aerogel blankets from our previous study was used [20]. Therefore, the thermal conductivity coefficient, k_{eff}, is calculated using Eq. (14), which is calculated from the presented model in ref. [20]:

$$k_{eff} = k_{cond.} + k_{rad.} \quad (14)$$

Fig. 12 and Fig. 13 demonstrate the variation of the thermal resistances as a function of compressive load for four different samples, which are predicted well with the modeling. Results show that when the compression load was increased from 0.7 kPa to 4.5 kPa, the resistance decreased 8.5% for CZ and 9% for TW for 5 mm thick samples. These values for samples with higher thickness were 10% and 8.5% for CZ and TW, respectively. Hence, it can be concluded that thermal resistance reduction in aerogel blanket insulation can be as high as 8%, under ~7 kPa compression, which is only due to mechanical deformation, i.e. thickness reduction. For rock wool, cellulose and fiberglass were shown that the resistance reduction, from full thickness condition of 30 cm, after applying just about

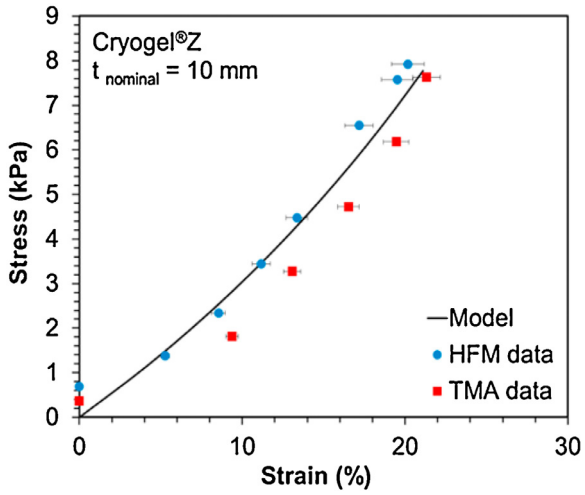

Fig. 9. Experimental stress-strain data and modeling result for CZ sample of 10 mm nominal thickness.

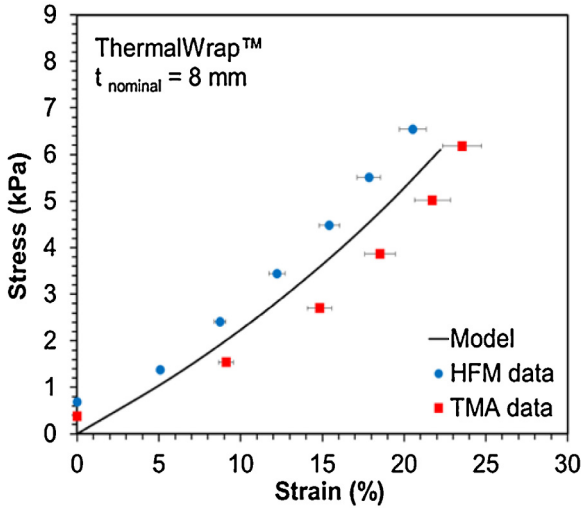

Fig. 10. Experimental stress-strain data and modeling result for TW sample of 5 mm nominal thickness.

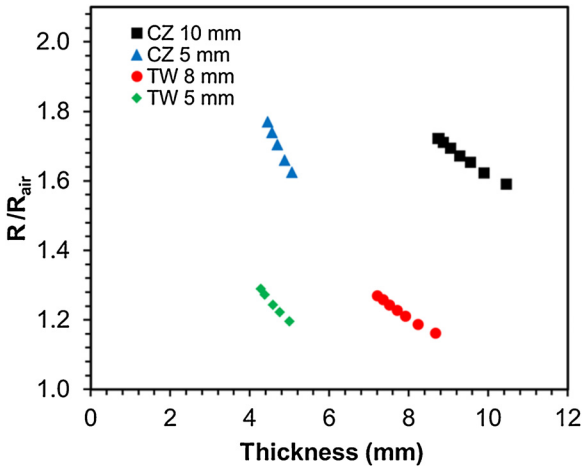

Fig. 11. Total resistance variation as a function of thickness.

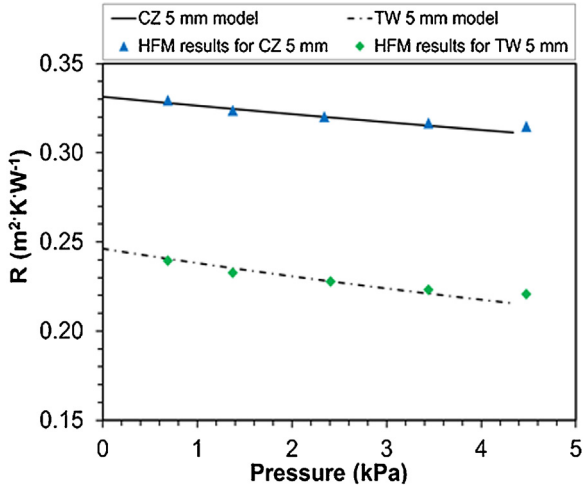

Fig. 12. Thermal resistance variation of CZ of 5 mm nominal thickness and TW of 5 mm nominal thickness at various compressive loads.

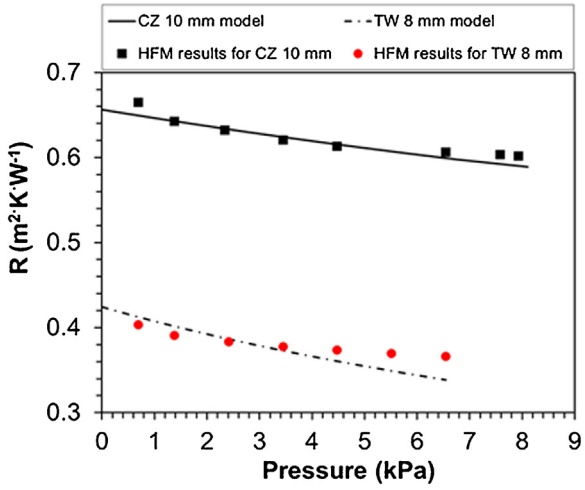

Fig. 13. Thermal resistance variation of CZ of 10 mm nominal thickness and TW of 8 mm nominal thickness at various compressive loads.

0.14 kPa load were 20%, 23% and 20%, respectively [7], which was much greater than the thermal resistance loss that occurs for aerogel blanket under similar condition. Hence, aerogel blankets are remarkably more efficient thermal insulation materials in terms of thermal performance and space occupation, considering the required thickness of conventional insulations for having almost the same thermal resistance as aerogel blankets, their deformation and thermal resistance loss under compression.

Additionally, the effects of loading history on deformation as well as thermal conductivity of the available samples were investigated. Presented in Fig. 14, the changes to the materials under repeated loading cycles between 0.7–2 kPa for thicker samples and 0.7–5 kPa for thinner ones were subtle, and the responses of the materials to compression became stable after ~10 cycles of mechanical deformation. Hysteresis in the HFM loading-unloading cycles indicated that plastic deformation occurred. This was attributed to the inelastic nature of aerogel blankets. Applying 20 compression-decompression cycles decreased the thickness of 10 mm CZ by 6% and decreased the thickness of 8 mm TW by 3.5%. The thermal conductivities of the samples decreased 4.7% and 1.7%, respectively. For the 5 mm samples, a thickness reduction of 2% for CZ and 1.5% for TW were observed along with thermal conductivity decreases of 0.6% and 0.5% for CZ and TW, respectively.

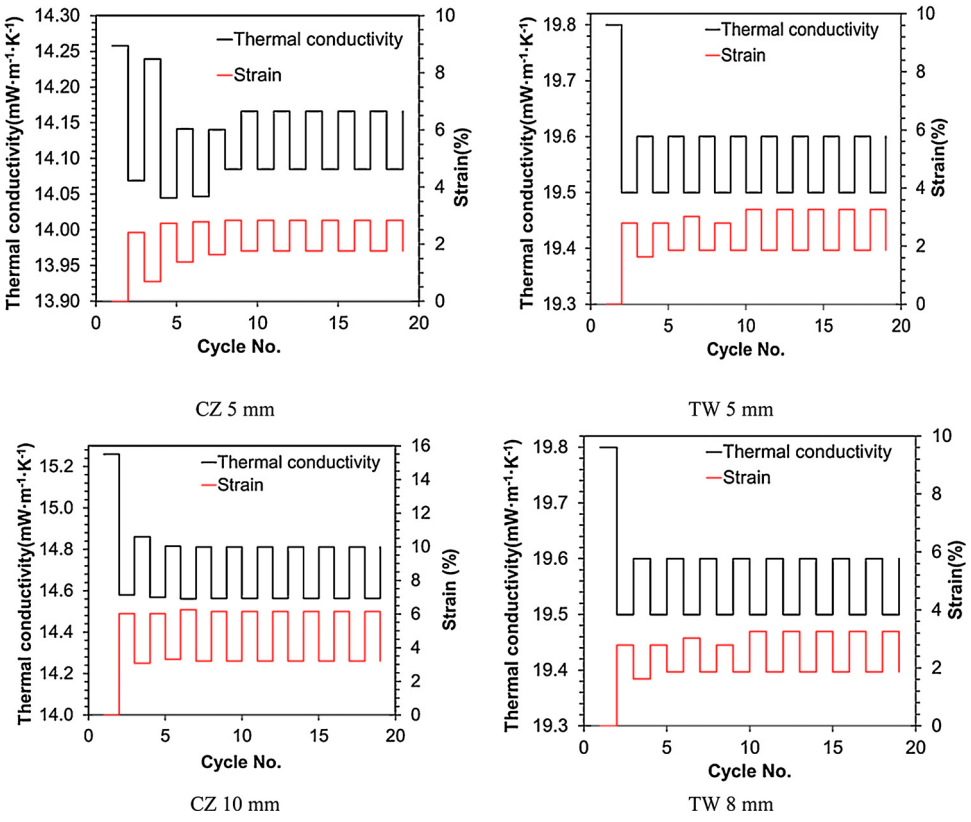

Fig. 14. Cycle test for load range of 0.7–2 kPa for thinner samples and 0.7–5 kPa for thicker ones.

5. Conclusion

In the present study, R-values of two types of commercially available aerogel blankets were measured using a minimum compressive load and several compressed conditions for two different thicknesses of each product. The effect of compression on the deformation and thermal resistance of the blankets was studied. The analytically predicted deformation of aerogel blanket under compression matched well with the experimental results from tests performed with a heat flow meter and a thermomechanical analyzer. The presented results showed small thermal resistance and thickness variations (maximum of 10% and 20% reduction, respectively) for all the samples under the maximum possible load of about 8 kPa and for cyclic loads (0.7–4.5 kPa).

Acknowledgment

The authors gratefully acknowledge the financial support of the Natural Sciences and Engineering Research Council of Canada (NSERC) through the Automotive Partnership Canada Grant No. APCPJ 401826-10. This work made use of the 4D LABS shared facilities supported by the Canada Foundation for Innovation(CFI), British Columbia Knowledge Development Fund (BCKDF), Western Economic Diversification Canada (WD), and Simon Fraser University (SFU). We also thank Mr. Sina Salari and Dr. Claire McCague for comments that greatly improved the manuscript.

References

[1] Natural Resources Canada (NRC), “Energy efficiency trends in Canada 1990–2009,” 2011.
[2] Statistics Canada, “Households and the environment: energy Use,” Ottawa, 2011.
[3] M.A. Aegerter, N. Leventis, M.M. Koebel, Aerogel Handbook, Springer, New York, 2011.
[4] C. Buratti, E. Moretti, E. Belloni, F. Agosti, Development of innovative aerogel based plasters: preliminary thermal and acoustic performance evaluation, Sustain 6 (9) (2014) 5839–5852.
[5] C.Y. Kim, J.K. Lee, B.I. Kim, Synthesis and pore analysis of aerogel-glass fiber composites by ambient drying method, Colloids Surf. A Physicochem. Eng. Asp. 313–314 (2008) 179–182.
[6] H. Maleki, L. Durães, A. Portugal, An overview on silica aerogels synthesis and different mechanical reinforcing strategies, J. Non. Cryst. Solids 385 (2014) 55–74.
[7] D.W. Yarbrough, J. ti. Wright, (1981). Reduction in the thermal resistance of loose fill insulation and fiberglass batts due to compression, Cookeville Tennessee.
[8] R.D. Adams, J.G. Hust, A round robin on apparent thermal conductivity of several loose-fill insulations, Insul. Mater. Test. Appl. (1990) 263–289 (ASTM STP 1030).
[9] R.S. Graves, D.W. Yarbrough, The effect of compression on the material R −value of fiberglass batt insulation, J. Therm. Insul. 15 (1992) 248–260.
[10] J.G. Symons, V. Clarke, R.E. ClarkePeirce, The thermal performance of several Australian fibrous insulating materials, Therm. Insul. bldg. Envs. 19 (July) (1995) 72–88.
[11] M. Kolich, P. Hoke, D. Dooge, M. Doroudian, E. Litovsky, J. Kleiman, Influence of temperature and mechanical compression on thermophysical properties of car interior foam plastics insulation, J. Elastomers Plast. 46 (2) (2014) 132–143.
[12] E. Cuce, P.M. Cuce, C.J. Wood, S.B. Riffat, Optimizing insulation thickness and analysing environmental impacts of aerogel-based thermal superinsulation in buildings, Energy Build. 77 (2014) 28–39.
[13] N. Gupta, W. Ricci, Processing and compressive properties of aerogel/epoxy composites, J. Mater. Process. Technol. 198 (2008) 178–182.
[14] E.R. Bardy, J.C. Mollendorf, D.R. Pendergast, Thermal conductivity and compressive strain of aerogel insulation blankets under applied hydrostatic pressure, J. Heat Transfer 129 (2) (2007) 232.
[15] D. Shi, Y. Sun, J. Feng, X. Yang, S. Han, C. Mi, Y. Jiang, H. Qi, Experimental investigation on high temperature anisotropic compression properties of ceramic-fiber-reinforced SiO2 aerogel, Mater. Sci. Eng. A 585 (2013) 25–31.
[16] H. Wu, Y. Liao, Y. Ding, H. Wang, C. Peng, S. Yin, Engineering thermal and mechanical properties of multilayer aligned fiber-reinforced aerogel composites, Heat Transf. Eng. 35 (11–12) (2014) 1061–1070.
[17] A. Neugebauer, K. Chen, A. Tang, A. Allgeier, L.R. Glicksman, L.J. Gibson, Thermal conductivity and characterization of compacted, granular silica aerogel, Energy Build. 79 (2014) 47–57.
[18] L. Waguespack, (2013). Thermomechanical Analysis (TMA Q400EM/Q400 specifications).

[19] ASTM C518-10, (2010). Standard test method for steady-state thermal transmission properties by means of the heat flow meter apparatus, ASTM, International, West Conshohocken, PA.
[20] A. Hoseini, C. McCague, M. Andisheh-Tadbir, M. Bahrami, Aerogel blankets: from mathematical modeling to material characterization and experimental analysis, Int. J. Heat Mass Transf. 93 (2016) 1124–1131.
[21] "AZO Materials." [Online]. Available: http://www.azom.com/properties.aspx?ArticleID=764.
[22] "The engineering toolbox." [Online]. Available: http://www.engineeringtoolbox.com/young-modulus-d_417.html.
[23] "Thermal wrap data sheet," no. i. p. 2011, (2011).
[24] M. U. Temp, "Cryogel ® Z data sheet.".
[25] V. Norouzifard, M. Bahrami, Deformation of PEM fuel cell gas diffusion layers under compressive loading: an analytical approach, J. Power Sources 264 (2014) 92–99.